

RESEARCH ARTICLE | JUNE 11 2019

Modeling of mass transfer enhancement in a magnetofluidic micromixer FREE

Chandan Kumar; Majid Hejazian; Christopher From ; Suvash C. Saha  ; Emilie Sauret; Yuantong Gu; Nam-Trung Nguyen 



Physics of Fluids 31, 063603 (2019)

<https://doi.org/10.1063/1.5093498>



View
Online



Export
Citation

Articles You May Be Interested In

Magnetofluidic concentration and separation of non-magnetic particles using two magnet arrays

Biomicrofluidics (July 2016)

Effects of magnetic nanoparticles on mixing in droplet-based microfluidics

Physics of Fluids (March 2019)

Enhancing micromixing using external electric and magnetic fields

Physics of Fluids (August 2024)



Physics of Fluids

Special Topics Open
for Submissions

[Learn More](#)

Modeling of mass transfer enhancement in a magnetofluidic micromixer

Cite as: Phys. Fluids 31, 063603 (2019); doi: 10.1063/1.5093498

Submitted: 21 February 2019 • Accepted: 20 May 2019 •

Published Online: 11 June 2019



Chandan Kumar,¹ Majid Hejajian,² Christopher From,¹  Suvash C. Saha,^{3,a)}  Emilie Sauret,¹ Yuantong Gu,¹ and Nam-Trung Nguyen⁴ 

AFFILIATIONS

¹Chemistry Physics and Mechanical Engineering, Queensland University of Technology, Brisbane, QLD 4000, Australia

²ARC Centre of Excellence for Advanced Molecular Imaging, Department of Chemistry and Physics, La Trobe Institute for Molecular Sciences, La Trobe University, Melbourne, VIC 3086, Australia

³School of Mechanical and Mechatronic Engineering, Faculty of Engineering and Information Technology, University of Technology Sydney, Ultimo, NSW 2007, Australia

⁴Queensland Micro and Nanotechnology Centre, Griffith University, Brisbane, QLD 4111, Australia

^{a)}Author to whom correspondence should be addressed: Suvash.Saha@uts.edu.au

ABSTRACT

The use of magnetism for various microfluidic functions such as separation, mixing, and pumping has been attracting great interest from the research community as this concept is simple, effective, and of low cost. Magnetic control avoids common problems of active microfluidic manipulation such as heat, surface charge, and high ionic concentration. The majority of past works on micromagnetofluidic devices were experimental, and a comprehensive numerical model to simulate the fundamental transport phenomena in these devices is still lacking. The present study aims to develop a numerical model to simulate transport phenomena in microfluidic devices with ferrofluid and fluorescent dye induced by a nonuniform magnetic field. The numerical results were validated by experimental data from our previous work, indicating a significant increase in mass transfer. The model shows a reasonable agreement with experimental data for the concentration distribution of both magnetic and nonmagnetic species. Magnetoconvective secondary flow enhances the transport of nonmagnetic fluorescent dye. A subsequent parametric analysis investigated the effect of the magnetic field strength and nanoparticle size on the mass transfer process. Mass transport of the fluorescent dye is enhanced with increasing field strength and size of magnetic particles.

Published under license by AIP Publishing. <https://doi.org/10.1063/1.5093498>

I. INTRODUCTION

A micromixer is one of the most significant microfluidic devices that attracted a great deal of interest from the research community. Rapid mixing is important for many biological, chemical, and biochemical assays (Yang *et al.*, 2016; Zhu and Nguyen, 2012b). While passive micromixers purely rely on hydrodynamics and molecular diffusion, active micromixers require external energy such as electric, acoustic, optic, and magnetic fields to enhance mixing. The application of electric, acoustic, or optic fields often results in temperature rise, which is not desirable for sensitive samples such as cells or deoxyribonucleic acids (DNAs) (Nam-Trung and Zhigang, 2005; Yang *et al.*, 2016; and Zhu and Nguyen, 2012b). By contrast, magnetism provides advantages such as low cost, simplicity, contactless control, no induced heat, and independence of pH

level or ion concentration (Zhu and Nguyen, 2012b). Therefore, microfluidic devices controlled by magnetic forces have recently attracted increasing research activities (Yang *et al.*, 2016).

Several past studies demonstrated the enhancement of mixing with micromagnetofluidic techniques. Mao and Koser (2007) reported the manipulation of a ferrofluid (FF) stream with local alternating magnetic fields. The device could enhance mass transport significantly using low-voltage excitation. Tsai *et al.* (2009) and Fu *et al.* (2010) investigated the mixing phenomena experimentally between ferrofluid and water using a permanent magnet. The results showed that rapid mixing between ferrofluid and water could be achieved by placing permanent magnets in a suitable location. Mixing efficiency may reach 90%, which is significantly higher than that of molecular diffusion. Zhu and Nguyen (2012b) reported the mixing phenomena caused by the interaction

between a uniform magnetic field and a ferrofluid in a circular microfluidic chamber. Both studies used an electromagnet to generate the magnetic field. The authors showed that a mixing efficiency as high as 90% can be achieved instantaneously at a relatively low magnetic field of less than 10 mT. [Feng et al. \(2016\)](#) presented enhanced mixing by introducing Lagrangian chaos through electro-osmosis (EO) or induced charge electro-osmosis (ICEO) in an eccentric annulus. They found that the created Lagrangian chaos resulted in rapid mixing than pure EO or ICEO. [Zhu and Nguyen \(2012b\)](#) showed that both the flow rate and the viscosity affect the mixing process. [Parada and Zimmerman \(2006\)](#) used a magnetohydrodynamic model to analyze the interaction of a conductive fluid in both electric and magnetic fields using the Galerkin finite element method (FEM). [Li et al. \(2018\)](#) conducted several experiments on magnetic induced self assembly using mixed magnetic multiphase fluids comprised of silica microspheres. [Chen et al. \(2017\)](#) employed a multiphysics numerical model to investigate the sedimentation of two nonmagnetic particles in a magnetic fluid subjected to a magnetic field. Most of the previous works mentioned above did not report any numerical study and did not use diamagnetic dye for tracing the mass transport. Detailed numerical simulation provides better insight into the effect of different process parameters such as magnetic field strength, distances of the channel from magnet, concentration, and to optimize the design of the microchannel.

[Zhigang et al. \(2004\)](#) presented a 2D mixing model based on pure diffusion, i.e., with no disturbance induced by external fields. The authors reported both linear and nonlinear models with a diffusion coefficient as a function of the concentration and discovered that the nonlinear model fitted experimental data well. [Wang et al. \(2008\)](#) numerically investigated a magnetic particle driven micromixer with a pair of external electromagnets. The authors studied the effects of various design parameters such as the applied magnetic field strength and the operating frequency. [Wen et al. \(2009\)](#) presented a simple micromixer using ferrofluids and AC electromagnet. A mixing efficiency of 95% was achieved within 2 s. [Cao et al. \(2015\)](#) studied an active mixer based on a hybrid gradient magnetic field generated by a permanent magnet and an electromagnet. The magnet system generates an alternating uniform magnetic field. The hybrid magnetic field allowed for a mixing efficiency of 97%–99%. The authors also developed a numerical model, which was, however, not validated by experimental data. [Zhu and Nguyen \(2012a\)](#) investigated experimentally and numerically the spreading phenomena caused by the interaction between a uniform magnetic field and a magnetic fluid in microchannels. In this work, the magnetic force is compensated by a correction factor to fit the simulation results with experimental data. The correction factor is 1000 for ferrofluid core and 100 for a ferrofluid-cladding case. Thus, this numerical model could only provide qualitative insight into the phenomenon. [Zhu and Nguyen \(2012a\)](#) reported the spreading of ferrofluid core with oil as cladding streams. The experimental results showed a strong spreading phenomenon at a higher magnetic field strength and a lower flow rate ratio. However, the numerical model needed a correction factor of approximately 1000 to match experimental data.

Specifically, numerical modeling is needed to obtain a quantitative description of ferrofluid flow, spreading, and focusing in the presence of a magnetic field. Simulations are also helpful to

understand the phenomenon of magnetofluidic spreading, and its applications ([Zhaomeng et al., 2015](#)). [Wang et al. \(2015\)](#) reported a numerical model that agreed well with their experimental data, without the use of any correction factor. However, the evolution of magnetofluid spreading over time and the relative importance of the factors governing the phenomenon was not reported. All the above models do not consider the susceptibility of ferrofluid as a function of the concentration of the magnetic nanoparticle. Therefore, the models might provide an erroneous prediction. Some models were affected by numerical diffusion which needs to be addressed before more accurate and quantitative simulation data can be obtained ([Zhu and Nguyen, 2012b](#)). Recently, the diffusion enhancement using a magnetic field for nonmagnetic species such as fluorescent dye has been investigated experimentally by [Hejazian et al. \(2016\)](#). However, the numerical simulation for mass transfer enhancement of nonmagnetic species induced by nonuniform magnetic field has not been investigated.

The present study aims to develop a comprehensive numerical model to investigate mass transfer enhancement of ferrofluid and fluorescent dye using a nonuniform magnetic field. A comprehensive numerical method for understanding the transport phenomena of multiple species in a micromagnetofluidic system is lacking. In addition, the numerical model will serve as a design tool of micromagnetofluidic platforms for fluid handling applications such as mixing and particle separation. The model was validated against previous experimental data ([Hejazian et al., 2016](#)) and provided a good agreement between simulation and experimental data. Furthermore, a parametric analysis is conducted to study the effect of nanoparticle size and distance of the channel from the magnets on mixing. The paper is structured into three sections. Section II presents the numerical simulation along with their boundary and initial conditions. Section III reports the results, discussion, and parametric analysis. Section IV finally concludes the paper.

II. NUMERICAL MODEL

This section presents the general governing equations with specific assumptions for each physics involved in the simulation of the magnetofluidic mass transport phenomena. Then, necessary initial and boundary conditions and input parameters required for developing the model are also presented and discussed in details.

A. Geometry and material

[Figure 1](#) shows the schematic of the microchannel and the magnet setup. The microchannel has a height of $H = 50 \mu\text{m}$, a width of $2W = 500 \mu\text{m}$, and a length of $L = 12 \text{ mm}$, three inlets, a straight rectangular mixing channel, and a single outlet.

We considered a two-dimensional (2D) geometry with a shallow channel approximation to compensate the three-dimensional (3D) effect. A common 2D approximation often fails to give the correct results, where the depth of the channel is much smaller than the width as 2D approximations exclude the boundaries, which have a great effect on the flow. The shallow channel approximation overcomes this problem by considering the effect of the unaccounted boundaries of a 2D geometry ([Bruus, 2008](#)). This approximation

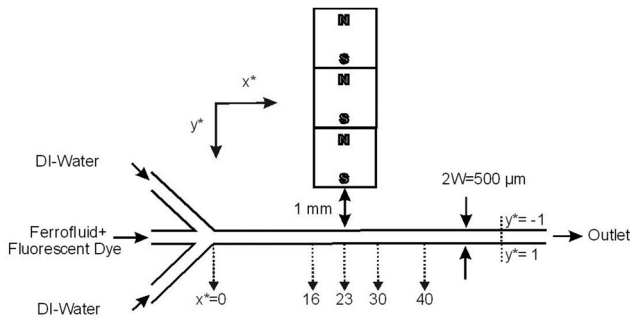


FIG. 1. Schematic of the microchannel and magnet setup. [Reproduced with permission from Hejazian, M., Phan, D.-T., and Nguyen, N.-T., "Mass transport improvement in microscale using diluted ferrofluid and a non-uniform magnetic field," RSC Adv. 6(67), 62439–62444 (2016). Copyright 2016 The Royal Society of Chemistry.]

adds a drag force term [shown in Eq. (1)] as volume force to the fluid flow equation to represent the resistance that the parallel boundaries place on the flow (Xu et al., 2013)

$$\vec{F}_u = -12 \frac{\mu_f \vec{u}_f}{H^2}, \quad (1)$$

where H is the channel height, \vec{u}_f is the velocity field (m/s), and μ_f is the dynamic viscosity of the fluid (Pa s).

The water-based ferrofluid (EMG707, Ferrotec) diluted to 20% volume concentration was used for the core stream. De-ionized (DI) water is introduced as sheath flow through the other two inlets. An amount of 0.05 g of fluorescein sodium salt (acid yellow, Sigma-Aldrich Co.) was dissolved in 20 ml of DI-water for visualization. The fluids were delivered using three precision syringe pumps (SPM100, SIMTech Microfluidics Foundry). Three 3.2-mm × 3.2-mm × 3.2-mm Neodymium-Iron-Boron (NdFeB) permanent magnets (B222, K&J Magnetics, Inc.) provide the magnetic field for the experiment. More details of the experimental method can be found in our previous paper (Hejazian et al., 2016).

B. Governing equations

1. Fluid flow

Because the Reynolds number in a typical microfluidic device is relatively small ($Re < 100$), the flow can be considered laminar (Bruus, 2008; Xu et al., 2013). With a Reynolds number on the order of 1, we can use Stokes flow to describe the system, which is also known as creeping flow. Under this condition, nonlinear inertial force, $\rho_f(\vec{u}_f \cdot \nabla \vec{u}_f)$, can be neglected (Bruus, 2008; Xu et al., 2013). Therefore, combining the shallow channel approximation and creeping flow, the incompressible steady-state Navier-Stokes equations become

$$\nabla \left[-PI + \mu_f \left(\nabla \vec{u}_f + (\nabla \vec{u}_f)^T \right) \right] + \vec{F} - \vec{F}_\mu = 0, \quad (2)$$

$$\nabla \cdot (\rho_f \vec{u}_f) = 0, \quad (3)$$

where ρ_f is the density of the fluid, \vec{u}_f is the velocity field (m/s), μ_f is the dynamic viscosity of the fluid (Pa s), \vec{F}_μ is the drag force as

described in Eq. (1), P is the pressure (N/m²), I is the identity matrix, and \vec{F} is the volume force (N/m²).

The effective density of ferrofluid, ρ_f , is given by

$$\rho_f = (1 - \phi)\rho_w + \phi\rho_{np}, \quad (4)$$

where ρ_{np} is the density of nanoparticles, ρ_w is the density of water, and ϕ is the volume fraction of magnetic nanoparticles (MNPs).

The effective dynamic viscosity of the mixture can be calculated by (Brinkman, 1952; Rabbi et al., 2016)

$$\mu_f = \mu_w \left(\frac{1}{(1 - \phi)^{0.25}} \right), \quad (5)$$

where μ_w is the viscosity of DI water.

The body force \vec{F} in Eq. (2) represents the Kelvin body force (i.e., the force that a magnetic fluid experiences in a spatially nonuniform magnetic field per unit volume) and can be calculated as (Strek, 2008)

$$\vec{F} = (\vec{M} \cdot \nabla) \vec{B}, \quad (6)$$

where \vec{B} is the magnetic flux density distribution (W/m²), \vec{M} is the magnetization which can be calculated from magnetic field physics discussed in Sec. II B 2.

2. Magnetic field

The magnetic field is calculated by solving Maxwell equations for the set of permanent magnets. The following equations govern the magnetic field for a permanent magnet:

$$\nabla \cdot \vec{B} = 0, \quad (7)$$

$$\vec{H} = -\nabla V_m. \quad (8)$$

The magnetization relation $\vec{B} = \mu_0(\vec{H} + \vec{M})$ for the magnets and relative permeability relation $\vec{B} = \mu_0\mu_r\vec{H}$ were used (Fateen and Magdy, 2015), where H is the magnetic field distribution (A/m), B is the magnetic flux density distribution (W/m²), M is the magnetization, and V_m is the magnetic scalar potential. The μ_0 and μ_r terms represent the vacuum permeability and relative permeability, respectively.

3. Transport of diluted species

Transport of diluted species is used to calculate the concentration, c (mol/l), where the spatial and temporal variation of the MNPs, c_{np} , and solution inside the microchannel is described by the convective–diffusive equation

$$\vec{u}_{np} \cdot \nabla c_{np} + \nabla \cdot (-D_{eff,np} \nabla c_{np}) = R_{np} \quad (9)$$

and similarly, the variation of the fluorescent dye concentration, c_{fd} , is described by

$$\vec{u}_{fd} \cdot \nabla c_{fd} + \nabla \cdot (-D_{eff,fd} \nabla c_{fd}) = R_{fd}, \quad (10)$$

where c_{np} is the concentration, \vec{u}_{np} is the velocity (m/s), and $D_{eff,np}$ is the effective diffusivity coefficient (m²/s) of the MNPs, and R is the consumption and generation with subscripts np and fd indicating MNP and fluorescent dye, respectively. There is no consumption and generation of particles for both MNP and fluorescent dye in this case, and, therefore, R_{np} and R_{fd} are set to zero.

The total velocity of a particle, u_p , is the vector summation of hydrodynamic velocity, u , obtained from Eq. (2) and a drift velocity, (u_{mag}) induced by the magnetic force

$$\vec{u}_p = \vec{u} + \vec{u}_{mag,np}. \quad (11)$$

The drift velocity can be calculated from the magnetic force exerted on the material given by

$$\vec{u}_{mag,np} = \frac{\vec{F}_{mag,np}}{6\pi\eta_w r_{np}}. \quad (12)$$

Here, $\vec{F}_{mag,np}$ is the magnetic force (N), η_w is the dynamic viscosity of water (Pa s), and r_{np} is the radius of the MNPs (m).

The magnetic force $\vec{F}_{mag,np}$ exerted on a particle can be evaluated from the total moment on the particle and applied magnetic field by the following equation:

$$\vec{F}_{mag,np} = (\vec{m} \cdot \nabla) \vec{B}, \quad (13)$$

where \vec{m} is the total moment on the particle, $\vec{m} = V_p \vec{M}$, which depends on its volume, V_p , and the volume magnetization, \vec{M} . Here, $\vec{M} = \Delta\chi \vec{H}$ and $\Delta\chi$ is the volumetric magnetic susceptibility difference between the particle, χ_p , and the surrounding buffered fluid medium, χ_f . Therefore, the magnetic force exerted on a particle can then be determined by the strength and gradient of the applied magnetic field, $\vec{B} = \mu_0 \vec{H}$, yielding to (Plouffe *et al.*, 2011; Tarn *et al.*, 2013)

$$\vec{F}_{mag,np} = \frac{V_p(\chi_p - \chi_f)(\vec{B} \cdot \nabla) \vec{B}}{\mu_0}, \quad (14)$$

where μ_0 is the permeability of vacuum $4\pi \times 10^{-7} \text{ TmA}^{-1}$.

Typically, forces on magnetic particles range from a few piconewton to a few tens of piconewton (Pamme, 2006). The term $\Delta\chi = \chi_p - \chi_f$ can be positive or negative, i.e., the particle can be repelled from or attracted to the high magnetic field gradient.

For a diluted ferrofluid, the effective diffusivity, $D_{eff,np}$, of the MNPs can be obtained using the Stokes–Einstein equation (Probstein, 2005) given by the following equation (Ranjan *et al.*, 2011):

$$D_{eff,np} = \frac{k_B T}{3\pi\eta_w d_{np}}. \quad (15)$$

Here, k_B is the Boltzmann constant ($1.38062 \times 10^{-23} \text{ J/K}$), T is the temperature (K), and d_{np} is the diameter of the nanoparticles (m). The numerator, $k_B T$, of Eq. (15) represents an estimate of the translational kinetic energy of a particle, whereas the denominator of the equation represents viscous drag force, in Newtons (Tarn *et al.*, 2014).

The nonlinear equation for diffusion coefficient had better prediction capability for diffusive mixing in the microchannel (Zhigang *et al.*, 2004). Datta (2007) and Ni (1997) proposed the diffusion coefficient to be a function of concentration that can be expressed as a nonlinear exponential function. Therefore, a similar nonlinear equation of diffusion coefficient as a function of MNP volume fraction is considered in this study and expressed by

$$D_{eff,fd} = 10^{-9} e^{(2+50\phi_{np})}. \quad (16)$$

The coefficients of the exponential term were obtained by adjusting the fluorescent dye concentration with experimental data.

C. Initial conditions, boundary conditions, and input parameters

The volumetric flow rate for sheath flow was $\dot{V}_{sh} = 30 \mu\text{l/min}$ and that of core flow was $\dot{V}_c = 2 \mu\text{l/min}$. The inlet boundary conditions were set at a constant velocity for the sheath flow and core flow calculated as follow.

For the sheath flow, $\vec{v}_{sh} = \frac{\dot{V}_{sh}}{A_{sh}}$, where A_{sh} is the cross section area of the sheath channel.

For the core flow, $\vec{v}_c = \frac{\dot{V}_c}{A_c}$, where A_c is the cross section area of the core channel.

The exit was set at the outflow condition, i.e., zero pressure, $p = 0$.

No slip condition was employed at the walls, i.e., $\vec{u} = 0$.

In this study, the permanent magnets are assumed to be magnetized indefinitely in the absence of an applied field (Gonzalez, 2009). The inflow condition was used for the concentration of MNPs and fluorescent dye.

1. Input parameters

The input parameters of the model are listed in Table I. The other variables which are not listed are discussed in this section.

TABLE I. List of input parameters for the model.

| Description | Value and unit | Reference |
|---|-------------------------------------|---|
| Density of ferrofluid, ρ_{ff} | 1100 $\frac{\text{kg}}{\text{m}^3}$ | Zhu <i>et al.</i> (2014) and Zhu and Nguyen (2012b) |
| Viscosity of ferrofluid, η_{ff} | $5 \times 10^{-3} \text{ Pa s}$ | Zhu <i>et al.</i> (2014) and Zhu and Nguyen (2012b) |
| Diameter of nanoparticles, d_{np} | 10 nm | |
| Volume fraction of nanoparticles, ϕ_{np} | 0.02 | |
| Density of NP (magnetite) Fe_3O_4 , ρ_{np} | 5.18 g/cm^3 | Blaney (2007) |
| Temperature, T | 25 $^\circ\text{C}$ | |
| Viscosity of water, μ_w | 0.000 89 Pa s | |
| Susceptibility of water, χ_w | -9.035×10^{-6} | |
| Relative permeability of magnet, μ_{mag} | 1.05 | Hejazian <i>et al.</i> (2015) |

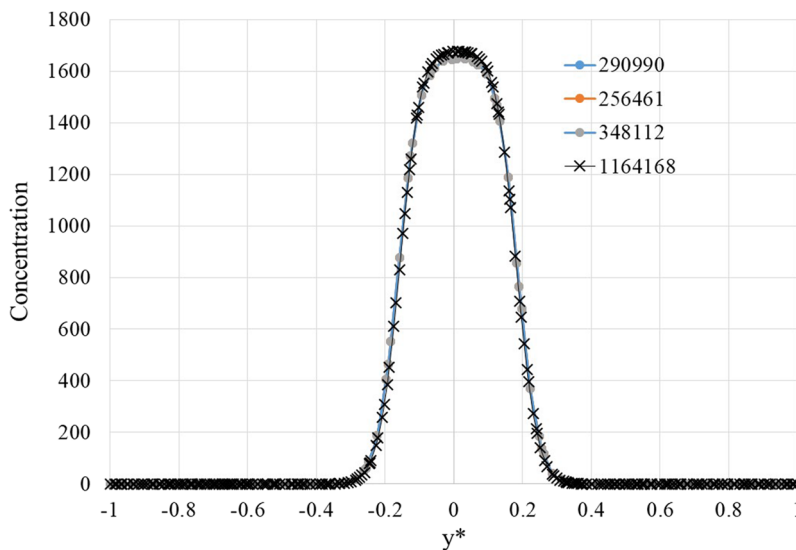


FIG. 2. Grid dependence test results.

The permeability of the ferrofluid is calculated using the Maxwell-Garnett theory (Garnett, 1904)

$$\mu_r = \mu_{r,m} \frac{1 + 2\phi\beta}{1 - \phi\beta}, \quad (17)$$

$$\beta = \frac{\mu_{r,p} - \mu_{r,m}}{\mu_{r,p} + 2\mu_{r,m}}, \quad (18)$$

where μ_r is the relative permeability of the ferrofluid, $\mu_{r,m}$ is the relative permeability of the continuous medium (water in this case), $\mu_{r,p}$ is the relative permeability of the magnetic nanoparticles of the ferrofluid, and β is the so-called magnetic contrast factor (López-López *et al.*, 2006).

D. COMSOL implementation

COMSOL Multiphysics 5.3 (COMSOL, Inc., USA) was used to solve the numerical model. Magnetic field (no currents) physics was used to simulate the permanent magnetic field. Creeping flow in the laminar regime was used for fluid flow simulation, and the transport of diluted species physics was used to calculate the concentration of nanoparticles and fluorescent dye. The solution of the magnetic field was taken as input for the fluid flow and the convective-diffusive transport. A grid dependency test was conducted with 256 461, 290 990, 348 112, and 1 164 168 elements and indicated that the results (concentrations) do not change noticeably with the number of selected elements (Fig. 2). The average mesh quality of all meshes tested was 0.9941. The mesh quality is sometimes referred to the minimum element quality where element quality is defined as $q = \frac{4\sqrt{3}A}{h_1^2 + h_2^2 + h_3^2}$, where A is the area, h_1 , h_2 , and h_3 are the side lengths of the triangular mesh. The mesh quality close to 1 is mostly ideal for a homogeneous material. Therefore, based on this grid dependency study, a mesh with a total of 290 990 triangular elements, which had a maximum element size of 10 μm and an average mesh quality of 0.9854, was chosen to investigate the fluid flow and concentration inside the channel.

III. RESULTS AND DISCUSSION

A. Experimental validation of the model

The correct estimation of the magnetic field is essential for predicting the fluid flow and nanoparticle concentration as the convective transport of nanoparticle and body force are affected by the magnetic field. Figure 3 shows a comparison between the simulated and experimental magnetic flux densities. The simulation results agree well with the experimental data. Note that the microchannel is located between 1 and 1.5 mm distances from the magnet, where the simulation matches better with experimental data.

Figure 4 shows the concentration distribution of the fluorescent dye inside the microchannel. Closer to the inlet, dye concentration is highest at the center of the channel because of hydrodynamic

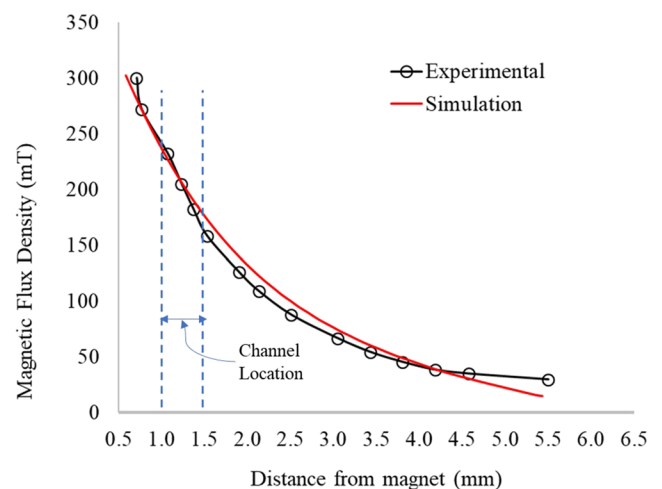


FIG. 3. Magnetic flux density vs distance from the surface of the magnet.

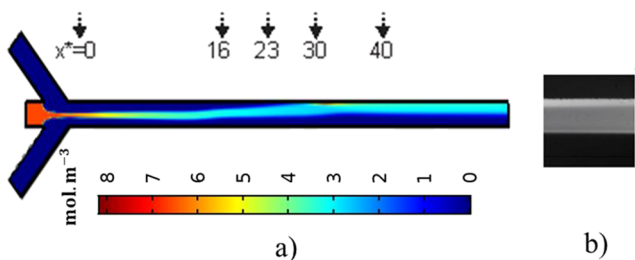


FIG. 4. Qualitative concentration diagram from our (a) simulation and (b) experiment at $x^* = 40$. Experimental results (b) are reproduced with permission from Hejazian, M., Phan, D.-T., and Nguyen, N.-T., "Mass transport improvement in microscale using diluted ferrofluid and a non-uniform magnetic field," RSC Adv. 6(67), 62439–62444 (2016). Copyright 2016 The Royal Society of Chemistry.

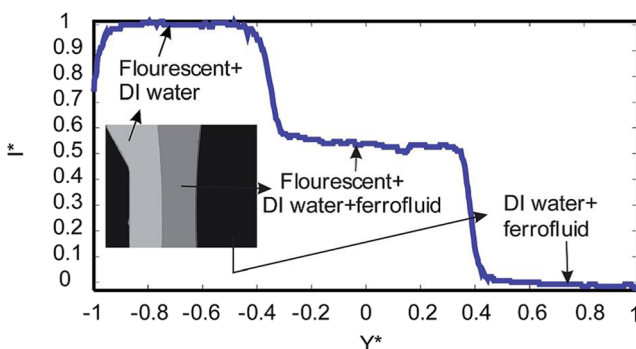


FIG. 5. Experimental intensity calibration extracted from Hejazian *et al.* (2016). [Reproduced with permission from Hejazian, M., Phan, D.-T., and Nguyen, N.-T., "Mass transport improvement in microscale using diluted ferrofluid and a non-uniform magnetic field," RSC Adv. 6(67), 62439–62444 (2016). Copyright 2016 The Royal Society of Chemistry.]

focusing with the sheath flows. However, the dye concentration downstream is higher on the upper half of the channel due to the enhanced transport caused by the attraction of MNPs in the ferrofluid toward the magnets and the subsequent induced magneto-convective secondary flow (Hejazian and Nguyen, 2017; 2016). The

secondary flow carries fluorescent dye molecules along with convective transport. The secondary flow changes the velocity field and nanoparticles travel toward the magnets. The consequence of this phenomenon is the higher transport of dye molecules from the core stream to the upper sheath stream. Both experimental and simulation show a similar pattern. The experimental result [Fig. 3(b)] shows that there is a narrow brighter stream near the upper wall of the channel, which corresponds to a higher concentration of dye at $x^* = 40$ of the simulation, where $x^* = x/W$ is the dimensionless position along the x -direction and normalized by the channel width W .

To better compare with the experimental results, the numerical data were postprocessed carefully to correspond to the recorded normalized fluorescence intensity from experiments of our previous study (Hejazian *et al.*, 2016) by considering the concentration of the fluorescent dye and ferrofluid (FF) and the intensity calibration from the experiments. The dye and FF concentrations were calculated using Eqs. (9) and (10), respectively. These concentrations were then normalized by their maximum value in the whole field for each cross section along x^* . The normalized concentrations of dye and FF were denoted by C_{dye}^* and C_{FF}^* , respectively. It is possible to relate the normalized numerical concentration to the normalized intensity calibration from the experiments (Hejazian *et al.*, 2016) (Fig. 5). In the core flow, the fluid mixture contains 20% vol. FF and 80% vol. fluorescent dye in DI-water, where the corresponding calibration of Fig. 4 indicates an intensity concentration of $I^* = 0.55$. Given that the volume fraction of dye is 80% and a corresponding 80% intensity. Therefore, FF reduces the intensity by $I^* = 0.8 - 0.25 = 0.55$.

The corresponding fluorescence intensity can be easily defined through the normalized concentration of the different components with respect to the total fluid and then subtracting one from the other, $I^* = |C_{dye}^* - C_{FF}^*|$.

It can be seen that the concentration distribution is almost Gaussian with the peak at center (Fig. 6). Experiments also indicate that similar concentration distribution and the magnetic field has no effect on concentration distribution at the inlet (Hejazian *et al.*, 2016). As expected, the flow-focusing configuration results in a concentration of MNPs to be highest at the center of the inlet. Consequently, the core appears darker at the

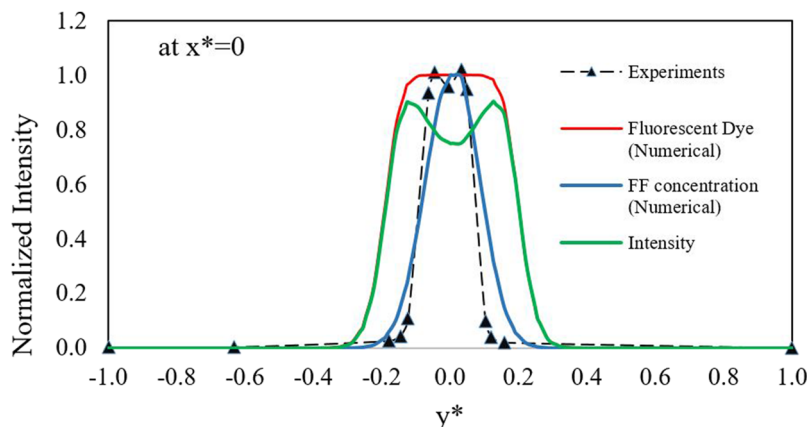


FIG. 6. Comparison between normalized concentration distribution of fluorescent dye and normalized light intensity from experiments at $x^* = 0$ (inlet).

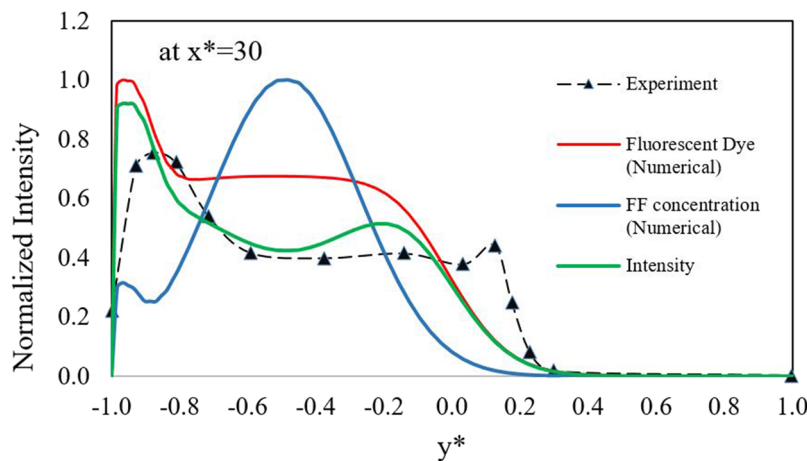


FIG. 7. Comparison between normalized concentration distribution of fluorescent dye and normalized light intensity from experiments at $x^* = 30$.

center of the channel, creating the saddle shape of the fluorescence intensity. This phenomenon can be observed in both the simulation and experiment. However, numerical results predict a broader width for both dye and FF concentrations, with both of the saddle peaks underpredicted. The width of the FF concentration matches with the experiments. However, the fluorescent dye concentration is broader due to the higher diffusion coefficient of the much smaller dye molecules. The percentage of error near the peak is about 9%–20%; however, since the percentage of error was calculated based on normalized values (<1), this calculation is very sensitive.

Figure 7 shows the concentration distribution of fluorescent dye from simulation and experimental light intensity at $x^* = 30$. The concentration profile shifted toward the left-hand side of the graph (i.e., upper half of the channel) due to magnetoconvection in both the experiment and simulation.

The spreading width of the core stream from the experiment and simulation is shown in Fig. 8. The simulation closely matches with the experimental values with a R^2 value of 0.98. The spreading

width or mass transport increases along the length of the channel and reaches a value of half width (peak) at $x^* = 30$.

In conclusion, the simulation can reasonably predict the trend at of concentration distribution at various locations such as at $x^* = 0$ (Fig. 6) and $x^* = 30$ (Fig. 7). The prediction of spreading width of fluorescent dye is even more accurate, as shown in Fig. 8.

B. Parametric analysis

The following parametric study was conducted to examine how the concentration distribution of fluorescence dye varies with one or more input parameters. Since the distance of the channel from the magnets and size of nanoparticles are the two key factors that affect the concentration distribution of dye, the parametric analysis of these two factors was considered.

Figure 9 shows the two-dimensional concentration distribution of the fluorescent dye with magnets positioned located 1 mm and 1.5 mm away from the microchannel. With a 1-mm distance, the dye concentration can reach the top wall of the channel due to higher magnetic field strength. By contrast, the dye core has not reached the top wall with a 1.5-mm distance. Therefore, the simulation could be helpful to identify the optimum distance between the magnet and the microchannel. One interesting observation from the simulation is that the width of the core becomes wider with an increasing distance. The core dye concentration is not significantly affected near the inlet of the channel. This observation obtained from the numerical study agrees well with the experimental results obtained by Hejajian *et al.* (2016). The result shows that the core stream remains narrow at the inlet and slightly increases until $x^* = 16$. Beyond $x^* = 16$, the dye concentration disperses and becomes wider.

Figure 10 shows the normalized dye concentration at $x^* = 23$ (top subplot) and $x^* = 30$ (bottom subplot) for 1-mm, 1.25-mm, and 1.5-mm distance between the magnets and the microchannel. The concentrations are plotted against normalized width [$y^* = y/W$ (Fig. 1)] where 0 to -1 refers to the upper half of the channel and 0 to $+1$ refers to the lower half of the channel. It is apparent that for $x^* = 30$, the dye concentration is higher near the upper wall of the channel compared to $x^* = 23$ as the dye is shifted more along the length on the downstream.

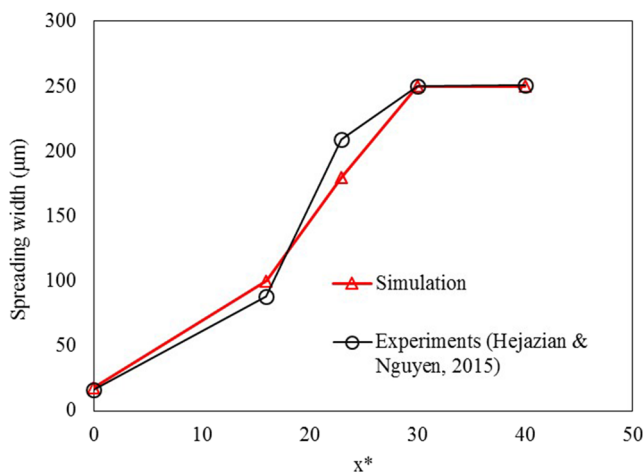


FIG. 8. Spreading widths of dye and FF.

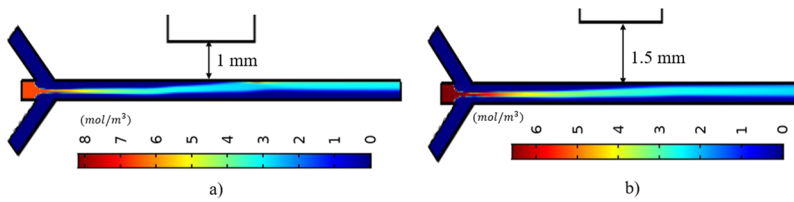


FIG. 9. Concentration distribution of the fluorescent dye in the channel for (a) 1 mm and (b) 1.5 mm distance of the magnet.

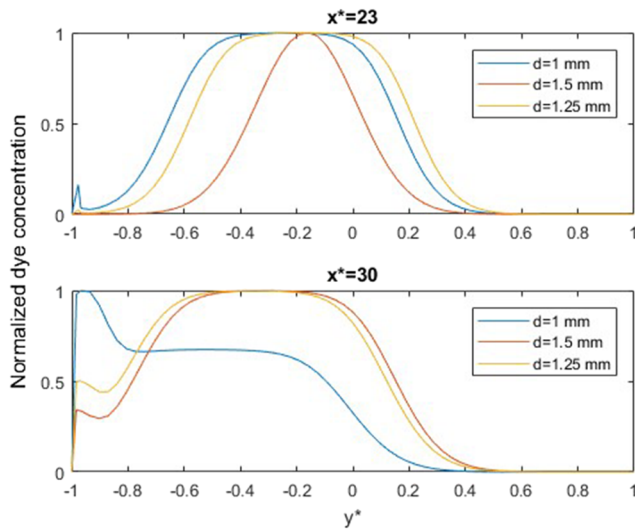


FIG. 10. Fluorescent dye concentration distribution in the channel for 1-mm, 1.25-mm, and 1.5-mm distance for $x^* = 30$ and $x^* = 23$.

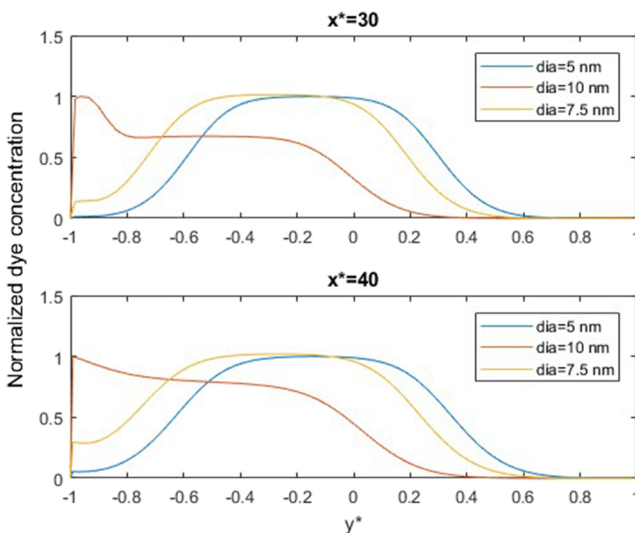


FIG. 11. The concentration of fluorescent dye along channel length for magnetic nanoparticle with diameters of 10 nm, 7.5 nm, and 5 nm.

For both $x^* = 23$ and 30 , the 1-mm distance allows the dye core to shift more toward the upper half of the channel compared to the larger distances. However, the width of the dye core remains almost same for 1.25-mm and 1.5-mm distances at $x^* = 30$. Although the core flow does not shift significantly at $x^* = 23$, the spreading width changes significantly with distance. Thus, decreasing the distance between the channel and magnets can significantly enhance mass transfer. At $x^* = 30$ and $d = 1$ mm, the dye concentration is highest near the wall. This is probably due to the accumulation of dye or ferrofluid at the wall.

Since the force exerted by the external magnet depends on the nanoparticle size, therefore, Fig. 11 shows the effect of the size on spreading. The larger particles experience more volume force according to Eq. (14). Therefore, the dye concentration with the 10-nm particle is higher near the upper wall of the channel (Fig. 11). This is more apparent for the downstream regime of the flow, i.e., for $x^* > 30$. For instance, at $x^* = 40$ (bottom figure), the 5-nm particle concentrated curve is bell shape with the highest concentration in the center of the core flow. Whereas at the same location ($x^* = 40$), the dye spread more toward the upper half of the channel, having the highest concentration near the wall for 10-nm particles. A similar pattern was observed for $x^* = 30$ and 10-nm particle, however, with a plateau near $y^* = -0.5$ and highest concentration near the wall. Therefore, for separation applications, the nanoparticle size could be chosen depending on the channel length using our numerical model.

IV. CONCLUSION

The present study develops a numerical model to investigate mass transfer enhancement phenomena of MNPs and fluorescent dye under nonuniform magnetic field. We demonstrated that the core stream with the MNPs of the ferrofluid and fluorescent dye near the inlet spreads into the upper sheath stream due to magnetoconvection. The spreading of the core stream reached a maximum concentration at $x^* > 30$. With the numerical model, we investigated the effect of distance between the magnet and the microchannel and the size of the MNPs of the ferrofluid. Increasing the distance between the magnets and the microchannel decreases the magnetic field strength and prevents the fluorescent dye from reaching the upper wall. By contrast, increasing the size of the MNPs in the ferrofluid enhances the transport of the fluorescent dye significantly. The present simulation results agree well with experimental data from our previous work. The numerical model presented in this paper could be employed for designing and optimizing magnetofluidic micromixers, gradient generators,

and magnetophoretic separators. Future works should focus on quantifying appropriate diffusion coefficient of MNPs and fluorescent dye to improve the prediction of the concentration of dye and nanoparticle.

ACKNOWLEDGMENTS

N. T. Nguyen acknowledges funding support from the Australian Research Council through the ARC linkage grant (No. LP150100153) and the ARC DP grant (No. DP180100055).

REFERENCES

- Blaney, L., *Magnetite (Fe_3O_4): Properties, Synthesis, and Applications* (Lehigh Preserve, 2007), Vol. 15-2007, Paper 5.
- Brinkman, H., "The viscosity of concentrated suspensions and solutions," *J. Chem. Phys.* **20**(4), 571 (1952).
- Bruus, H., *Theoretical Microfluidics* (Oxford University Press, New York, 2008).
- Cao, Q., Han, X., and Li, L., "An active microfluidic mixer utilizing a hybrid gradient magnetic field," *Int. J. Appl. Electromagn. Mech.* **47**(3), 583–592 (2015).
- Chen, M., Li, X., Niu, X., Li, Y., Khan, A., and Yamaguchi, H., "Sedimentation of two non-magnetic particles in magnetic fluid," *Acta Phys. Sin.* **66**, 164703 (2017).
- Datta, A. K., "Porous media approaches to studying simultaneous heat and mass transfer in food processes. II: Property data and representative results," *J. Food Eng.* **80**(1), 96–110 (2007).
- Fateen, S.-E. K. and Magdy, M., "Three dimensional simulation of negative-magnetophoretic filtration of non-magnetic nanoparticles," *Chem. Eng. Res. Des.* **95**, 69–78 (2015).
- Feng, H., Neng Wong, T., Che, Z., and Marcos, "Chaotic micromixer utilizing electro-osmosis and induced charge electro-osmosis in eccentric annulus," *Phys. Fluids* **28**, 062003 (2016).
- Fu, L. M., Tsai, C. H., Leong, K. P., and Wen, C. Y., "Rapid micromixer via ferrofluids," *Phys. Procedia* **9**, 270–273 (2010).
- Garnett, J. C. M., "Colours in metal glasses and in metallic films," *Philos. Trans. R. Soc., A* **203**(359-371), 385–420 (1904).
- Gonzalez, L. A., *Negative Magnetophoresis of Submicron Species in Magnetic Nanofluids* (Massachusetts Institute of Technology, 2009).
- Hejazian, M., Li, W., and Nguyen, N.-T., "Lab on a chip for continuous-flow magnetic cell separation," *Lab Chip* **15**(4), 959–970 (2015).
- Hejazian, M. and Nguyen, N. T., "Magnetofluidic concentration and separation of non-magnetic particles using two magnet arrays," *Biomicrofluidics* **10**(4), 044103 (2016).
- Hejazian, M. and Nguyen, N.-T., "Magnetofluidics for manipulation of convective heat transfer," *Int. Commun. Heat Mass Transfer* **81**, 149–154 (2017).
- Hejazian, M., Phan, D.-T., and Nguyen, N.-T., "Mass transport improvement in microscale using diluted ferrofluid and a non-uniform magnetic field," *RSC Adv.* **6**(67), 62439–62444 (2016).
- Li, X., Niu, X.-D., Li, Y., and Chen, M.-F., "Self-assembly of silica microparticles in magnetic multiphase flows: Experiment and simulation," *Phys. Fluids* **30**(4), 040905 (2018).
- López-López, M. T., Kuzhir, P., Laci, S., Bossis, G., González-Caballero, F., and Durán, J. D. G., "Magnetorheology for suspensions of solid particles dispersed in ferrofluids," *J. Phys.: Condens. Matter* **18**(38), S2803 (2006).
- Mao, L. and Koser, H., "Overcoming the diffusion barrier: Ultra-fast micro-scale mixing via ferrofluids," in paper presented at the Transducers 2007—2007 International Solid-State Sensors, Actuators and Microsystems Conference, 10–14 June 2007.
- Nam-Trung, N. and Zhigang, W., "Micromixers—A review," *J. Micromech. Microeng.* **15**(2), R1 (2005).
- Ni, H., *Multiphase Moisture Transport in Porous Media under Intensive Microwave Heating* (Cornell University, 1997).
- Pamme, N., "Magnetism and microfluidics," *Lab Chip* **6**(1), 24–38 (2006).
- Parada, J. H. L. and Zimmerman, W. B., "The numerical simulation of a magneto-hydrodynamic DC microdevice based on the finite element method," *Courses Lect. - Int. Cent. Mech. Sci.* **466**, 167 (2006).
- Plouffe, B. D., Lewis, L. H., and Murthy, S. K., "Computational design optimization for microfluidic magnetophoresis," *Biomicrofluidics* **5**(1), 013413 (2011).
- Probstein, R. F., "Transport in fluids," in *Physicochemical Hydrodynamics* (John Wiley and Sons, Inc., 2005), pp. 9–30.
- Rabbi, K. M., Saha, S., Mojumder, S., Rahman, M. M., Saidur, R., and Ibrahim, T. A., "Numerical investigation of pure mixed convection in a ferrofluid-filled lid-driven cavity for different heater configurations," *Alexandria Eng. J.* **55**, 127 (2016).
- Ranjan, G., Ashok, S., and Ishwar, K. P., "Magnetic-particle-based microfluidics," in *Microfluidics and Nanofluidics Handbook* (CRC Press, 2011), pp. 433–484.
- Strek, T., *Finite Element Simulation of Heat Transfer in Ferrofluid* (Intech Open Access Publisher, 2008).
- Tarn, M. D., Lopez-Martinez, M. J., and Pamme, N., "On-chip processing of particles and cells via multilaminar flow streams," *Anal. Bioanal. Chem.* **406**(1), 139–161 (2014).
- Tarn, M. D., Peyman, S. A., and Pamme, N., "Simultaneous trapping of magnetic and diamagnetic particle plugs for separations and bioassays," *RSC Adv.* **3**(20), 7209–7214 (2013).
- Tsai, T.-H., Liou, D.-S., Kuo, L.-S., and Chen, P.-H., "Rapid mixing between ferro-nanofluid and water in a semi-active Y-type micromixer," *Sens. Actuators, A* **153**(2), 267–273 (2009).
- Wang, Y., Zhe, J., Chung, B. T., and Dutta, P., "A rapid magnetic particle driven micromixer," *Microfluid. Nanofluid.* **4**(5), 375–389 (2008).
- Wang, Z., Varma, V. B., Xia, H. M., Wang, Z. P., and Ramanujan, R. V., "Spreading of a ferrofluid core in three-stream micromixer channels," *Phys. Fluids* **27**(5), 052004 (2015).
- Wen, C.-Y., Yeh, C.-P., Tsai, C.-H., and Fu, L.-M., "Rapid magnetic microfluidic mixer utilizing AC electromagnetic field," *Electrophoresis* **30**(24), 4179–4186 (2009).
- Xu, X., Li, Z., and Nehorai, A., "Finite element simulations of hydrodynamic trapping in microfluidic particle-trap array systems," *Biomicrofluidics* **7**(5), 054108 (2013).
- Yang, R.-J., Hou, H.-H., Wang, Y.-N., and Fu, L.-M., "Micro-magnetofluidics in microfluidic systems: A review," *Sens. Actuators, B* **224**, 1–15 (2016).
- Zhaomeng, W., Varma, V. B., Wang, Z. P., and Ramanujan, R. V., "Tuning magnetofluidic spreading in microchannels," *J. Micromech. Microeng.* **25**(12), 124001 (2015).
- Zhigang, W., Nam-Trung, N., and Xiaoyang, H., "Nonlinear diffusive mixing in microchannels: Theory and experiments," *J. Micromech. Microeng.* **14**(4), 604 (2004).
- Zhu, G.-P., Hejazian, M., Huang, X., and Nguyen, N.-T., "Magnetophoresis of diamagnetic microparticles in a weak magnetic field," *Lab Chip* **14**(24), 4609–4615 (2014).
- Zhu, G.-P. and Nguyen, N.-T., "Magnetofluidic spreading in microchannels," *Microfluid. Nanofluid.* **13**(4), 655–663 (2012a).
- Zhu, G.-P. and Nguyen, N.-T., "Rapid magnetofluidic mixing in a uniform magnetic field," *Lab Chip* **12**(22), 4772–4780 (2012b).